



Review

Research Progress on Rashba Effect in Two-Dimensional Organic–Inorganic Hybrid Lead Halide Perovskites

Junhong Guo ¹, Jinlei Zhang ², Yunsong Di ^{3,*} and Zhixing Gan ^{3,4,*}

¹ College of Electronic and Optical Engineering & College of Flexible Electronics (Future Technology), Nanjing University of Posts and Telecommunications, Wenyuan Road 9, Nanjing 210023, China; jhguo@njupt.edu.cn

² School of Physical Science and Technology, Suzhou University of Science and Technology, Suzhou 215009, China; zhangjinlei@usts.edu.cn

³ Center for Future Optoelectronic Functional Materials, School of Computer and Electronic Information, Nanjing Normal University, Nanjing 210023, China

⁴ College of Materials Science and Engineering, Qingdao University of Science and Technology, Qingdao 266042, China

* Correspondence: diyunsong@njnu.edu.cn (Y.D.); zxgan@njnu.edu.cn (Z.G.)

Abstract: The Rashba effect appears in the semiconductors with an inversion–asymmetric structure and strong spin-orbit coupling, which splits the spin-degenerated band into two sub-bands with opposite spin states. The Rashba effect can not only be used to regulate carrier relaxations, thereby improving the performance of photoelectric devices, but also used to expand the applications of semiconductors in spintronics. In this mini-review, recent research progress on the Rashba effect of two-dimensional (2D) organic–inorganic hybrid perovskites is summarized. The origin and magnitude of Rashba spin splitting, layer-dependent Rashba band splitting of 2D perovskites, the Rashba effect in 2D perovskite quantum dots, a 2D/3D perovskite composite, and 2D-perovskites-based van der Waals heterostructures are discussed. Moreover, applications of the 2D Rashba effect in circularly polarized light detection are reviewed. Finally, future research to modulate the Rashba strength in 2D perovskites is prospected, which is conceived to promote the optoelectronic and spintronic applications of 2D perovskites.

Keywords: Rashba effect; photoluminescence; 2D perovskites; optoelectronics and spintronics



Citation: Guo, J.; Zhang, J.; Di, Y.; Gan, Z. Research Progress on Rashba Effect in Two-Dimensional Organic–Inorganic Hybrid Lead Halide Perovskites. *Nanomaterials* **2024**, *14*, 683. <https://doi.org/10.3390/nano14080683>

Academic Editor: Michael Saliba

Received: 22 March 2024

Revised: 9 April 2024

Accepted: 13 April 2024

Published: 16 April 2024



Copyright: © 2024 by the authors. Licensee MDPI, Basel, Switzerland. This article is an open access article distributed under the terms and conditions of the Creative Commons Attribution (CC BY) license (<https://creativecommons.org/licenses/by/4.0/>).

1. Introduction

Organic–inorganic hybrid lead halide perovskites (OILHPs) have attracted significant interest in the past years due to their outstanding performance as solar absorbers in photovoltaics [1–5]. The long carrier lifetime of photogenerated carriers is a crucial factor for excellent optoelectronic performance [6]. An extraordinarily long carrier lifetime ($\tau \geq 1 \mu\text{s}$) and a substantial carrier diffusion length ($L_D \geq 5 \mu\text{m}$) have been measured in polycrystalline perovskite thin films with moderate mobility ($\mu \approx 1\text{--}100 \text{ cm}^2 \text{ V}^{-1} \text{ s}^{-1}$), which is drastically lower than that of other conventional semiconductors, such as GaAs ($\mu \approx 500 \text{ cm}^2 \text{ V}^{-1} \text{ s}^{-1}$). However, the physical mechanism behind the long carrier lifetime is still elusive [7–11]. The mainstream investigation attributes it to the low trap density [12,13], which may lead to a significant suppression in nonradiative recombination, thus greatly prolonging the carrier's lifetime. However, further research has found that, in perovskites with relatively high defect density, the carrier lifetime does not significantly decrease [14]. Therefore, the correlation between carrier lifetime and defect density in perovskite is not definite. Currently, other models, such as high defect tolerance [15–17], photon recycling [18,19], weak electron–phonon coupling [20–23], the presence of ferroelectric domains [24,25], the formation of polarons, and the screening of band-edge charges [26], have been proposed to rationalize the long carrier lifetime of perovskites. However, after years of laborious

exploration, there are still some inherent limitations and inconsistencies in the above-mentioned models.

Among them, the Rashba effect is also considered to be one of the most essential reasons for the long carrier lifetime [27–29]. The Rashba effect was proposed in the 1950s, which reveals spin splitting in noncentrosymmetric semiconductors [30,31]. For ordinary semiconductors, the dispersion of the conduction band minimum (CBM) electrons and valence band maximum (CBM) holes can be described as a spin-degenerate parabolic energy band,

$$E(\mathbf{k}) = \hbar^2 \mathbf{k}^2 / 2m^* \quad (1)$$

where \mathbf{k} is the electron wavevector, \hbar is the reduced Planck constant, and m^* is the effective mass of electrons (or holes). However, if the semiconductor lacks inversion symmetry, and meanwhile there is strong spin-orbit coupling, an effective magnetic field $\Omega(\mathbf{k})$ appears (Figure 1a), which lifts the degeneracy of the carrier spin states within each band [32]. Thus, when the Rashba effect occurs, the spin-degenerate parabolic band splits into two spin-polarized sub-bands deviating from the symmetric center of the Brillouin zone (Figure 1b,c).

$$E_{\pm}(\mathbf{k}) = \hbar^2 \mathbf{k}^2 / 2m^* \pm \alpha_R |\mathbf{k}| \quad (2)$$

α_R is the Rashba splitting constant.

$$\alpha_R = \frac{2E_R}{k_R} \quad (3)$$

Figure 1c shows that the Rashba effect has two important characteristics, namely, energy band splitting and in-plane spin splitting. E_R and k_R are the energy difference and momentum offset between the vertex of the energy curve and the \mathbf{k} origin at the high-symmetry point, respectively. The strength of the Rashba effect is usually characterized by the Rashba constant α_R .

Due to the different orbital compositions of the conduction band and valence band, the splitting degrees of the CBM and VBM are not equal. Therefore, the splitting will make the carrier recombination in perovskite exhibit features similar to indirect bandgap, thereby reducing the carrier recombination rate. In addition, because the conduction band and valence band have opposite spin helicity, carrier recombination is spin forbidden, which further reduces the electron-hole recombination rate. Optical selection rules for interband transitions at the band gap are plotted in Figure 1d. The Rashba effect not only provides a possible explanation for the long carrier lifetime in perovskites but also enables effective control and manipulation of the polarized spins in spintronic devices. Apart from the research on conventional optoelectronics areas, such as solar cells, LEDs, and photodetectors [33–36], one of the exciting research directions on lead halide perovskites would be spintronics-related technology.

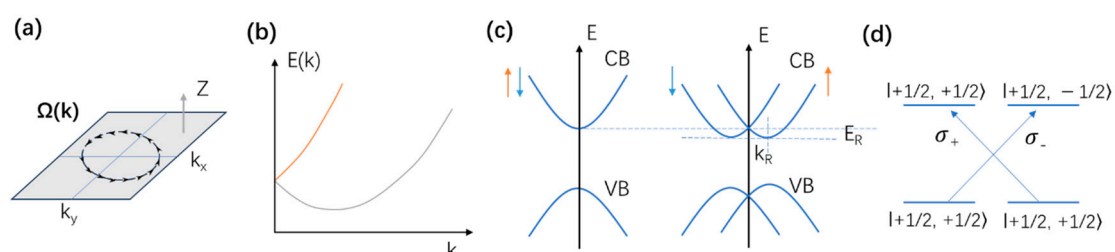


Figure 1. (a) Effective magnetic field $\Omega(\mathbf{k})$ induced by the Rashba effect showing the variation of the direction at a fixed value of $|\mathbf{k}|$. (b) Energies of the spin eigenstates as a function of the in-plane wave vector. (c) The electron dispersion relation shows a doubly degenerate parabolic band at $\mathbf{k} = 0$ subject to Rashba spin splitting, fostering two parabolic bands with opposite spins (arrows). (d) Optical selection rules for interband transitions at the band gap.

The Rashba effect is considered one of the most essential reasons for the long carrier lifetime of OILHPs. Moreover, the photoelectronic properties of OILHPs that can be regulated by the magnitude of the Rashba effect. Thus, the Rashba effect in 2D OILHPs has attracted increasing research interest. In this mini-review, the recent research progress on the Rashba effect in 2D perovskites is summarized. Several important aspects of the Rashba effect in 2D perovskites, including the origin and magnitude, layer dependence in 2D perovskite, the Rashba effect in 2D perovskite quantum dots, 2D/3D composite, and van der Waals heterostructures, are included. In addition, circularly polarized light-detection applications based on the Rashba effect are discussed. Due to the limitation of scope, this review does not include all achievements related to this topic, and only a selection of representative examples is discussed. We hope this mini-review can further stimulate research enthusiasm on this important topic so that more insights into the fundamental understanding can be gained and more optoelectronic and spintronic applications can be developed.

2. Rashba Effect in Three-Dimensional (3D) Perovskites

It is generally believed that the crystal structure of three-dimensional OILHP (such as MAPbI₃, MA = methylamine) at room temperature is a tetragonal system (or cubic system or orthogonal system, depending on the material composition) with centrosymmetry. However, it has been found that the perovskite lattice does not have strict centrosymmetry [29]. The lead halide octahedron [MX₆]^{4−} in the perovskite lattice is slightly distorted [37], and the organic cation A⁺ also has a certain orientation in a rapidly rotating state [38,39]. These properties may disrupt the centrosymmetry of the perovskite lattice. In addition, there is strong spin-orbit coupling due to the presence of heavy elements, such as lead, tin, and iodine. The Rashba effect in perovskites is expected to be strong. Based on the above reasons, many theoretical studies predict a strong Rashba effect in perovskites [37,40]. For example, the spin-orbit coupling in MAPbI₃ causes a displacement of the conduction band energy level of more than 1 eV [41]. In addition, a few experimental studies also strongly support the occurrence of the Rashba effect in the compound [42,43]. A significant effort regarding the experimental observation of Rashba spin-splitting has been demonstrated by Giovanni and co-workers through spin-dependent circularly polarized pump-probe experiments [42]. Neisner et al. directly observed the split in the valence band by angle-resolved photoemission spectroscopy measurements [43].

3. Rashba Effect in Two-Dimensional Perovskites

Two-dimensional OILHPs are commonly known as the Ruddlesden–Popper (RP) phase [44–51] and the Dion–Jacobson (DJ) phase [52]. Taking RP-phase 2D perovskite as an example, its general chemical structure is (RNH₃)₂A_{n−1}M_nX_{3n−1} (*n* = 1, 2, 3, 4, ...), where RNH₃ is usually an organic group of aliphatic or aromatic alkylammonium, such as 2-phenylethylammonium (PEA) and *n*-butylammonium (*n*-BA), A is a monovalent organic cation, such as CH₃NH₃⁺ (abbreviated as MA⁺) and HC(NH₂)₂⁺ (abbreviated as FA⁺), and M is a divalent metal cation, mainly referring to lead Pb, X is a halide anion. The large organic cations (RNH₃⁺) separate the layers of the inorganic Pb-I network. And *n* represents the number of inorganic [MX₆]^{4−} octahedral structures in each period. The 2D OILHPs have attracted increasing research interest due to their special multi-quantum-well structures and excellent structural stability under ambient conditions [53,54].

Bychkov and Rashba proposed that the Rashba effect also appears in two-dimensional (2D) electron gas systems [55]. Thus, the Rashba effect has been extensively investigated in various 2D material systems, including III–V semiconductor heterostructures and topological insulators Bi₂Se₃ over the past few decades [56–58]. Nevertheless, Rashba splitting energy in these 2D structures is typically smaller than 10 meV, limiting the performance of spintronic devices based on these 2D materials [56–58]. The Rashba effect in 2D perovskites has also attracted extensive research attention. Density functional theory (DFT) calculation is an important tool for defining and demonstrating the existence of Rashba

splitting, as well as quantifying the structural symmetry, rotation, and distortion. For example, Zhai et al. showed the existence of Rashba splitting in the plane perpendicular to the 2D layer of $(\text{C}_6\text{H}_5\text{C}_2\text{H}_4\text{NH}_3)_2\text{PbI}_4$ based on the DFT calculations using local density approximation (LDA) in the form of ultrasoft pseudopotentials [59]. In more detail, the first-principles DFT calculations show that the breaking of inversion symmetry is caused by the displacement of the Pb atom from the octahedra center, which leads to the Rashba splitting. At temperatures below 110 K, the absorption spectrum in the photon energy range of 2.45 to 2.65 eV shows two step-like absorption edges, which are assigned as the 1s and 2s exciton energy at 2.38 and 2.53 eV, respectively (Figure 2a). Considering the band edge of $(\text{C}_6\text{H}_5\text{C}_2\text{H}_4\text{NH}_3)_2\text{PbI}_4$ at 2.57 eV (Figure 2b), 1s and 2s exciton binding energies are about 190 ± 4 meV and 45 ± 8 meV, respectively. The energy differences between δE_{ac} and δE_{bc} scales with $V^{2/3}$ indicate a Frank–Keldysh-type oscillatory feature at the continuum band edge (Figure 2c). From the electroabsorption spectrum and photoinduced absorption spectra of excitons and free carriers, they obtained a giant Rashba splitting in 2D $(\text{C}_6\text{H}_5\text{C}_2\text{H}_4\text{NH}_3)_2\text{PbI}_4$ thin film, with energy splitting of (40 ± 5) meV and a Rashba constant of (1.6 ± 0.1) eV·Å (Figure 2d) [59].

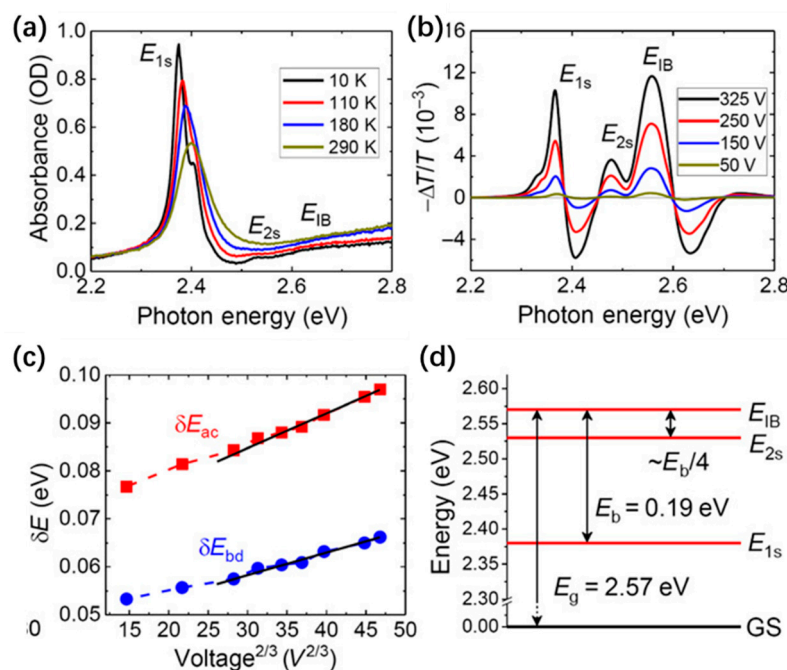


Figure 2. (a) Absorption spectra of $(\text{C}_6\text{H}_5\text{C}_2\text{H}_4\text{NH}_3)_2\text{PbI}_4$ film at various temperatures, which contains 1s and 2s exciton (labeled as E_{1s} and E_{2s} , respectively) and an interband (IB) transition. (b) Electroabsorption spectra of $(\text{C}_6\text{H}_5\text{C}_2\text{H}_4\text{NH}_3)_2\text{PbI}_4$ thin film measured at 45 K at various applied to electric fields. (c) Energy differences δE_{ac} and δE_{bc} plotted versus $V^{2/3}$. (d) Energy levels of the excitons and interband transition (IB) with respect to the ground state (GS) [59]. Reproduced with permission under Creative Common CC-BY 4.0 license.

In addition, Todd et al. investigated carrier dynamics in 2D $(\text{BA})_2\text{MAPb}_2\text{I}_7$ thin film by time-resolved circular dichroism techniques [60]. They revealed the presence of a Rashba spin splitting via the dominance of precessional spin relaxation induced by the Rashba effective magnetic field. The Rashba spin-splitting magnitude was extracted from simulations of the measured spin dynamics incorporating longitudinal optical-phonon and electron–electron scattering, yielding a value of 10 meV at an electron energy of 50 meV above the band gap, which is twenty times larger than that in GaAs quantum wells. Moreover, a Rashba splitting of 85 meV with a Rashba coefficient α_R of 2.6 eV Å was observed in an emergent 2D DJ phase $(\text{AMP})\text{PbI}_4$ (AMP = 4-(aminomethyl)piperidinium) [61]. Jana et al. introduced a structural chirality transfer across the organic–inorganic interface

in 2D perovskites using appropriate chiral organic cations [62]. The chiral spacer cations and their asymmetric hydrogen-bonding interactions with lead bromide-based layers cause symmetry-breaking helical distortions in the inorganic layers. The first-principles calculation predicts a substantial bulk of the Rashba–Dresselhaus spin-splitting in the inorganic-derived conduction band with opposite spin textures between R- and S-hybrids due to the broken inversion symmetry and strong spin-orbit coupling. The chirality transfer from one structural unit to another represents a promising approach to breaking symmetry that modulates the Rashba effect for spintronics and related applications. These findings indicated that 2D hybrid perovskites have great potential for applications in spintronics.

3.1. Origin and Magnitude of Rashba Spin Splitting in 2D RP Perovskites

Rashba spin splitting has been observed in multiple 2D OILHPs, yet with a significant variance in the magnitude of spin splitting [58–61]. However, the origin of the giant Rashba splitting remains elusive. The crucial role of the orientation of the organic cation in the 2D RP perovskite was explored by Kagdada et al. Their DFT calculation results revealed that the MA cation rotation imposes structural distortion in the inorganic PbI_6 layer, which then varies the structure and value of the electronic bandgap, charge density, and optical absorption. The strong spin–orbit coupling leads to a wide range of Rashba splitting parameters from 0.04 to 0.278 eV Å. The simulated optical absorption spectra showed that absorption edges for the different orientations of the MA molecule are not the same [63].

In addition, Zhou et al. obtained (AMP) PbI_4 DJ phase crystals by an economical aqueous method. They clarified the origin of the giant Rashba effect by temperature- and polarization-dependent photoluminescence (PL) results [64]. The strong temperature-dependent PL helicity indicates the thermally assisted structural distortion as the main origin of the Rashba effect, suggesting that valley polarization still preserves at high temperatures. The Rashba effect was further confirmed by the circular photogalvanic effect near the indirect bandgap (Figure 3).

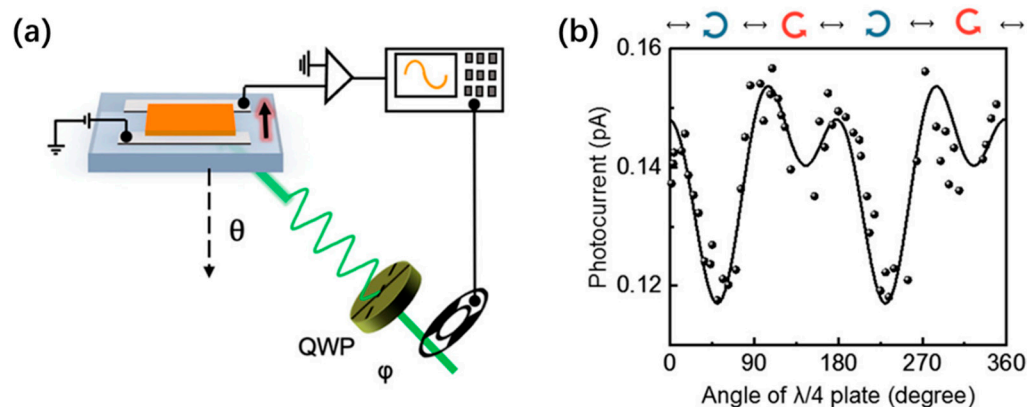


Figure 3. (a) Schematic illustration of the experimental setup for measurement of photogalvanic current. The φ indicates the angle between the fast axis of the quarter-wave plate (QWP) and the incident light polarization. The θ indicates the incident angle of excitation light. (b) Room temperature photogalvanic current of (AMP) PbI_4 versus QWP rotation angle φ , measured at $\theta = 60^\circ$ and excited via a 556 nm continuous laser [64]. Reproduced with permission. Copyright 2021, American Chemical Society.

In addition, organic–inorganic hybrid halide perovskites are susceptible to dynamic instabilities known as octahedral tilt, which involves a rigid rotation of the inorganic octahedral cages and can occur along any of the three Cartesian directions in the crystal with either in-phase or out-of-phase ordering [65]. While the phase transitions related to octahedral tilt have been thoroughly examined in 3D hybrid halide perovskites, their influence on hybrid 2D perovskites remains not fully comprehended. To gain insight into this puzzle, Shao et al. utilized scanning tunneling microscopy to directly visualize

the surface octahedral tilt in freshly exfoliated 2D RP perovskites across the homologous series [66]. The steric hindrance imposed by long organic cations is unlocked by exfoliation. The experimentally determined octahedral tilts from 2D RP-phase perovskites of $n = 1$ to $n = 4$ align closely with the out-of-plane surface octahedral tilts predicted by DFT calculations. The out-of-plane octahedral tilt of the exfoliated surface is correlated to the redshifted emission peak alongside the primary exciton in the PL spectra. Therefore, the Rashba spin splitting is attributed to the octahedral tilt [66].

3.2. Layer-Dependent Rashba Band Splitting in 2D Perovskites

It is very significant to reveal the impacts of surface termination and the number of inorganic layers on the amplitude of Rashba band splitting so as to enhance the understanding of the origin and extent of Rashba spin splitting in 2D RP-phase perovskites. Thus, research efforts were devoted to the layer-dependent Rashba band splitting in 2D perovskites. Singh et al. investigated Rashba spin splitting in 2D RP $(\text{BA})_2(\text{MA})_{n-1}\text{Pb}_n\text{I}_{3n+1}$ with both centrosymmetric ($n = 1$) and noncentrosymmetric ($n = 2$ and 3) structures, using first-principle calculations, polarization, and temperature-dependent PL spectroscopy [67]. They revealed the n -dependent Rashba spin splitting in 2D RP perovskites. When $n = 1$, a single metal halide octahedral layer is sandwiched between long BA^+ organic cations, Rashba spin splitting is the largest. As n increases, the Rashba spin splitting decreases. The large Rashba effect observed in the 2D RP perovskite of an $n = 1$ structure is attributed to the local distortion of the PbI_6 octahedron at the surface [67].

By using a combination of DFT calculations and time-resolved PL spectroscopy, Yin et al. compared the Rashba band splitting of the prototype 3D MAPbI_3 and the 2D RP perovskites [68]. They demonstrated that significant structural distortions associated with different surface terminations are responsible for the observed Rashba effect in 2D OILHPs. Interestingly, their calculation results indicated that the intrinsic Rashba splitting occurs in the perovskite crystals with an even number of inorganic layers ($n = 2$), in consistency with their longer PL lifetimes and ground-state bleaching recovery lifetimes. Whereas, when the number of inorganic layers is odd ($n = 1$ and $n = 3$), the Rashba effect of 2D RP perovskites absences (Figure 4). These findings elucidate the significant impact of the number of inorganic layers on the electronic properties of 2D perovskites, suggesting the controlling of the n value in 2D RP perovskites to design Rashba effects for spintronic applications.

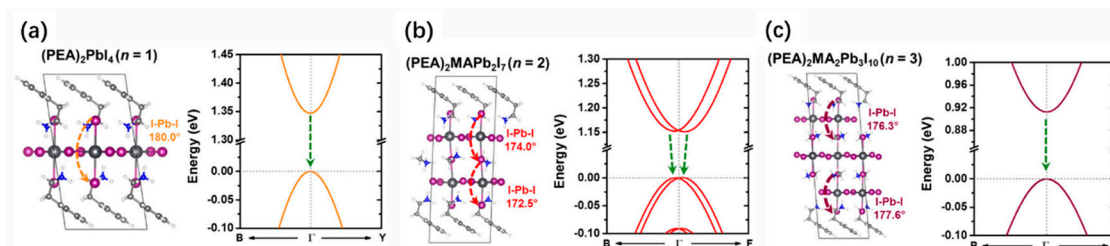


Figure 4. (a) Optimized crystal structures and electronic band structures of (a) $(\text{PEA})_2\text{PbI}_4$ ($n = 1$), (b) $(\text{PEA})_2\text{MAPb}_2\text{I}_7$ ($n = 2$), and (c) $(\text{PEA})_2\text{MA}_2\text{Pb}_3\text{I}_{10}$ ($n = 3$) [68]. Reproduced with permission. Copyright 2018, American Chemical Society.

In addition, Liu investigated the thickness-dependent structural distortion along with the Rashba splitting energy by using the DFT calculation [69]. Three types of OILHPs were compared to explore the effect of halogens and organic ligands. As the thickness increases, the structural distortion degree decreases. The Rashba splitting magnitude follows the same tendency. The 2D MAPbI_3 is less sensitive to thickness change compared to the 2D MAPbBr_3 or the 2D MAPbCl_3 . Furthermore, ligands and their orientations have dramatically different impacts on the Rashba splitting. The PEA ligands enhance the Rashba splitting magnitude, while the BA ligands have the converse effect. The partial charge-density analysis shows that the band edges are contributed to by a charge density

at a specific layer in the structure. Thus, they concluded that the Rashba effect is layer dependent in 2D HOIPs [69].

3.3. Rashba Effect in 2D Perovskite Quantum Dots

Because of the quantum confinement effect, the quantum dot usually shows fast radiative recombination, large exciton binding energies [70], and giant oscillator transition strengths [71]. Most theoretical descriptions of the Rashba effect on exciton fine structures were conducted in the weak-confinement regime, in which the exciton Bohr radius, r_B , is much smaller than the typical size of the nanocrystals. The Rashba effect was treated perturbatively, which is a valid approach, assuming $\alpha k \ll \frac{\hbar^2 k^2}{2m^*}$, where α_e and α_h are the Rashba coefficients in the conduction and valence bands, respectively, k is the typical quasi-momentum of exciton center-of-mass (COM) motion, and m^* is the effective mass of the COM motion. The momentum is $k \sim 1/R$ for an exciton confined in an NC with size R , so the perturbative approach is valid when $\alpha \ll \hbar^2/2m^*R$. This condition is clearly not satisfied in a large NC ($R \gg \hbar^2/2m^*\alpha$) or in NCs with enormously large Rashba coefficients. Thus, the Rashba effect in 2D perovskite quantum dots is elusive. To explore this question, Swift et al. constructed an effective mass model of excitons in 2D perovskite quantum dots, which covers the full range of NC sizes and Rashba strengths [72]. The fine structure and oscillator transition strengths of Rashba excitons confined in a 2D cylindrical quantum dot are quite unusual. One notable aspect of the energy-level structure is the proliferation of dark exciton states. These dark states in large quantum dots are also likely to be thermally populated even at quite low temperatures, reducing the radiative decay rate and, consequently, the PL quantum yield of these structures.

3.4. Rashba Effect in 2D/3D Composite Perovskite Films

Compared with common 2D perovskite, the 2D/3D composite perovskite may have a variety of gains, such as significant interface asymmetry and an effective energy-transfer process. On the one hand, the interface asymmetry can enhance the band splitting. On the other hand, energy transfer can be used to improve the photoresponse. These two effects make 2D/3D composite perovskite promising for opto-spintronic applications. The recent development of chiral 2D/three-dimensional (3D) composite perovskites offers a new opportunity to engineer the Rashba effect. Li et al. synthesized one pair of chiral 2D/3D composite perovskite [73]. The optical properties were studied by polarization-dependent femtosecond transient absorption (fs-TA) spectroscopy, which revealed that the chiral properties of organic cations were successfully transferred to the achiral part. The Rashba effect is significantly enhanced in the 2D/3D composite structures. The spintronic relaxation along with the Rashba effect in the 2D/3D composite structures will inspire the further development of the next generation of opto-spintronic devices.

3.5. Rashba Effect of Van Der Waals Heterostructures Based on 2D Perovskites

The van der Waals heterostructures based on different 2D materials enable innovative device engineering. A variety of van der Waals heterostructures have been developed based on 2D perovskites for optoelectronic applications. Thus, it is very significant to investigate the Rashba effect in van der Waals heterostructures. Singh et al. integrate an RP-phase 2D perovskites monolayer with another important family of 2D excitonic semiconductors, i.e., transition-metal dichalcogenides (TMDs) [67]. A combined effect of Rashba spin splitting in 2D RP perovskites and the strong spin-valley physics of monolayer TMDs can give rise to effective spin-valley polarization in the heterostructures using circularly polarized light (CPL) excitation. Thus, the 2D RP perovskite/TMD heterostructure provides an attractive material combination for investigating valleytronic phenomena, as it reduces fabrication complexity and sample-to-sample variance. Different 2D RP perovskites ($n = 1$ and 2) and monolayer WSe_2 s were coupled to form 2D vdW heterostructures. Robust interlayer excitons (IXs) in staggered type-II band-aligned heterostructures were observed (Figure 5). These IXs are strongly valley-polarized with exciton lifetimes longer than

the intralayer excitons in the constituent monolayer TMDs, suggesting the spin–valley-dependent optical selection rules to the IXs. This research broadens the scope for exploring spin–valley physics in heterogeneous stacks of 2D semiconductors. They also investigated a 2DRP-($n = 1$)/MoS₂ heterostructure with a broken type-III band alignment. In contrast, there is no interlayer charge transfer, thus the 2DRP/MoS₂ heterostructure does not show any IX emission.

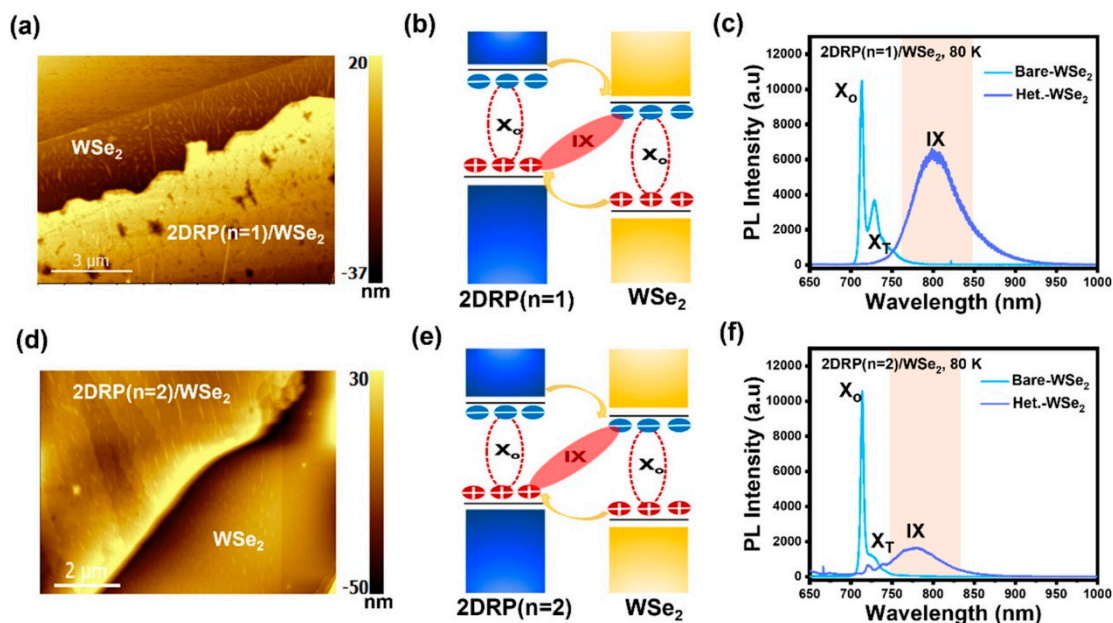


Figure 5. Topography (a,d), band structures (b,e), and PL spectra (c,f) of 2D RP ($n = 1$)/WSe₂ (a–c) and 2D RP ($n = 2$)/WSe₂ heterostructures (d–f) under 633 nm excitation. The type-II band alignment between monolayer WSe₂ and 2D RP perovskites leads to the formation of interlayer excitons [67]. Reproduced with permission. Copyright 2023, American Chemical Society.

3.6. Applications of 2D Rashba Effect in Circularly Polarized Light Detection

CPL is a special light beam, which consists of two spiral modes called chirality or handedness. Based on the rotation of the field vector, the CPL can either rotate counterclockwise (left handed, σ^+) or clockwise (right handed, σ^-) when observed from the direction opposite to the wave's propagation. Direct detection of CPL is a challenging task due to limited materials and ambiguous structure–property relationships that lead to low distinguishability of the light helicities. On the one hand, the circular photogalvanic effect is considered the most important experiment that confirms the presence of the Rashba effect in semiconductors. The circular photogalvanic effect has been demonstrated in a variety of materials with the Rashba effect, such as GaAs/AlGaAs multi-quantum wells, the polar semiconductor BiTeI, 2D transition-metal dichalcogenides, and topological insulators [74–77]. On the other hand, the Rashba effect in 2D perovskites provides new opportunities for dealing with the challenge of CPL detection.

Chiral 2D perovskites have been recently explored as the responsive component for the direct detection of CPL [78–84]. For example, Wang et al. inserted chiral organic ligands into the organic layers of 2D perovskites to obtain chiral (R-MBA)₂PbI₄ and (S-MBA)₂PbI₄. The in-plane photocurrent response generated by the CPL excitation of planar photoconductive devices shows a typical response of the chirality-induced circular photogalvanic effect that originates from the Rashba splitting in the electronic bands of these compounds, demonstrating the potential applications of chiral 2D perovskites in optoelectronic devices that are sensitive to the light helicity [85]. Similarly, Fan et al. report direct CPL detection by using a pair of 2D chiral perovskite ferroelectrics, (R/S-3AMP)PbBr₄ (3AMP = 3-(aminomethyl)-piperidine divalent cation) [86]. These 2D perovskites undergo a phase transition at 420 K

that is a combination of order–disorder and displacive ferroelectric transition. DFT calculations and circularly polarized light-excited PL measurements have confirmed the presence of the Rashba effect in these 2D chiral perovskites (Figure 6a–d). This effect results in spin selectivity, which can modulate the behavior of photogenerated charge carriers during transitions, recombination, and transfers. Single-crystal-based devices have been shown to directly detect CPL at 430 nm, with an on–off ratio of current higher than 1.7×10^3 and anisotropy factors of responsivity larger than 0.20 (Figure 6e). The enhanced CPL detection is attributed to the Rashba effect, which has a large Rashba coefficient of $0.93 \text{ eV} \cdot \text{\AA}$.

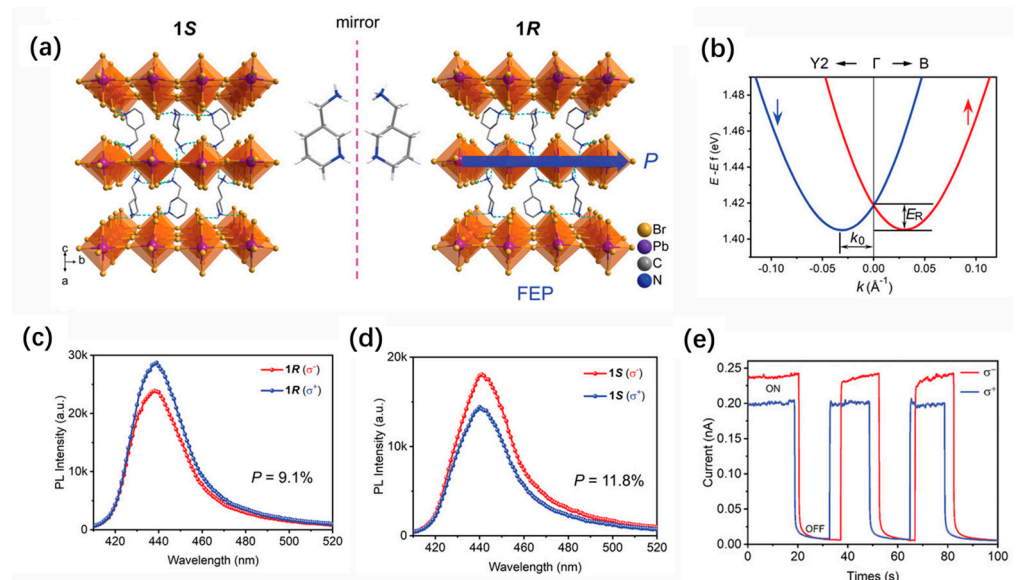


Figure 6. (a) Crystal structures of (S-3AMP)PbBr₄ (1S) and (R-3AMP)PbBr₄ (1R) in the ordered ferroelectric phase (FEP). (b) Rashba splitting band structure of 1R. (c,d) CPLEPL spectra of 1R (c) and 1S (d) upon L-CPL (σ^+) and R-CPL (σ^-) excitation at 395 nm. (e) Photocurrent differences upon L- and R-CPL irradiation at 430 nm [86]. Reproduced with permission. Copyright 2022, Wiley-VCH.

4. Conclusions and Outlook

In summary, this mini-review focuses on the Rashba effect in 2D perovskites. Recent research progress on the origin and extent of Rashba spin splitting, layer-dependent Rashba band splitting of 2D perovskites, the Rashba effect on 2D perovskite quantum dots, the Rashba effect in 2D/3D composite perovskite, and the Rashba effect in van der Waals heterostructures based on 2D perovskites are reviewed. In addition, applications of the 2D Rashba effect in circularly polarized light detection are included in this review.

Despite considerable reports on Rashba effects in 2D perovskites, the origin of Rashba spin splitting in 2D perovskites is still under debate. Future research efforts to investigate the impacts of the surface termination, the number of inorganic layers, the structure of organic spacers, the planar sizes, and the distortion of inorganic octahedrons on the magnitude of Rashba band splitting will not only gain more insight into the origin of Rashba effect in 2D perovskites but also inspire approaches to modulate the Rashba spin splitting. In addition, the relationship between charge-carrier dynamics and the Rashba effect in 2D perovskites is still to be established, so that the photoelectronic properties and photophysics of 2D perovskites can be effectively controlled by modulating the Rashba magnitude. Apart from the research on conventional optoelectronics areas, such as solar cells, LEDs, and photodetectors, one of the exciting research interests on 2D perovskites will be focused on spintronics-related technology. However, the current related research is still insufficient. In other words, there is plenty of room to design new spintronic devices based on 2D perovskites.

Author Contributions: Conceptualization, Z.G. and J.G.; writing—original draft preparation, J.G. and J.Z.; writing—review and editing, Z.G. and Y.D. All authors have read and agreed to the published version of the manuscript.

Funding: This work was supported by the Natural Science Foundation of Shandong Province (ZR2021YQ32), the China Postdoctoral Science Foundation (2023M740472), and the Taishan Scholars Program of Shandong Province (tsqn201909117), the National Natural Science Foundation of China (62004136).

Conflicts of Interest: The authors declare no conflict of interest.

References

1. Wang, F.; Chang, Q.; Yun, Y.; Liu, S.; Liu, Y.; Wang, J.; Fang, Y.; Cheng, Z.; Feng, S.; Yang, L.; et al. Hole-Transporting Low-Dimensional Perovskite for Enhancing Photovoltaic Performance. *Research* **2021**, *2021*, 9797053. [[CrossRef](#)] [[PubMed](#)]
2. Gottesman, R.; Zaban, A. Perovskites for Photovoltaics in the Spotlight: Photoinduced Physical Changes and Their Implications. *Acc. Chem. Res.* **2016**, *49*, 320–329. [[CrossRef](#)] [[PubMed](#)]
3. Huang, J.; Yuan, Y.; Shao, Y.; Yan, Y. Understanding the physical properties of hybrid perovskites for photovoltaic applications. *Nat. Rev. Mater.* **2017**, *2*, 17042. [[CrossRef](#)]
4. Aydin, E.; Allen, T.G.; De Bastiani, M.; Razaq, A.; Xu, L.; Ugur, E.; Liu, J.; De Wolf, S. Pathways toward commercial perovskite/silicon tandem photovoltaics. *Science* **2024**, *383*, eadh3849. [[CrossRef](#)] [[PubMed](#)]
5. Balaguera, E.H.; Bisquert, J. Accelerating the Assessment of Hysteresis in Perovskite Solar Cells. *ACS Energy Lett.* **2024**, *9*, 478–486. [[CrossRef](#)] [[PubMed](#)]
6. Maiti, A.; Pal, A.J. Carrier recombination in CH₃NH₃PbI₃: Why is it a slow process? *Rep. Prog. Phys.* **2022**, *85*, 024501. [[CrossRef](#)] [[PubMed](#)]
7. Ambrosio, F.; Wiktor, J.; De Angelis, F.; Pasquarello, A. Origin of low electron–hole recombination rate in metal halide perovskites. *Energy Environ. Sci.* **2018**, *11*, 101–105. [[CrossRef](#)]
8. Chen, T.; Chen, W.-L.; Foley, B.J.; Lee, J.; Ruff, J.P.C.; Ko, J.Y.P.; Brown, C.M.; Harriger, L.W.; Zhang, D.; Park, C.; et al. Origin of long lifetime of band-edge charge carriers in organic–inorganic lead iodide perovskites. *Proc. Natl. Acad. Sci. USA* **2017**, *114*, 7519–7524. [[CrossRef](#)] [[PubMed](#)]
9. Frost, J.M.; Butler, K.T.; Brivio, F.; Hendon, C.H.; van Schilfgaarde, M.; Walsh, A. Atomistic Origins of High-Performance in Hybrid Halide Perovskite Solar Cells. *Nano Lett.* **2014**, *14*, 2584–2590. [[CrossRef](#)]
10. Zhang, C.; Sun, D.; Vardeny, Z.V. Multifunctional Optoelectronic–Spintronic Device Based on Hybrid Organometal Trihalide Perovskites. *Adv. Electron. Mater.* **2017**, *3*, 1600426. [[CrossRef](#)]
11. Zhang, Z.; Long, R.; Tokina, M.V.; Prezhdo, O.V. Interplay between Localized and Free Charge Carriers Can Explain Hot Fluorescence in the CH₃NH₃PbBr₃ Perovskite: Time-Domain Ab Initio Analysis. *J. Am. Chem. Soc.* **2017**, *139*, 17327. [[CrossRef](#)] [[PubMed](#)]
12. Yamada, Y.; Nakamura, T.; Endo, M.; Wakamiya, A.; Kanemitsu, Y. Photocarrier Recombination Dynamics in Perovskite CH₃NH₃PbI₃ for Solar Cell Applications. *J. Am. Chem. Soc.* **2014**, *136*, 11610. [[CrossRef](#)] [[PubMed](#)]
13. Stranks, S.D.; Burlakov, V.M.; Leijtens, T.; Ball, J.M.; Goriely, A.; Snaith, H.J. Recombination Kinetics in Organic–Inorganic Perovskites: Excitons, Free Charge, and Subgap States. *Phys. Rev. Appl.* **2014**, *2*, 034007. [[CrossRef](#)]
14. Azarhoosh, P.; McKechnie, S.; Frost, J.M.; Walsh, A.; van Schilfgaarde, M. Research Update: Relativistic origin of slow electron–hole recombination in hybrid halide perovskite solar cells. *APL Mater.* **2016**, *4*, 091501. [[CrossRef](#)]
15. Steirer, K.X.; Schulz, P.; Teeter, G.; Stevanovic, V.; Yang, M.; Zhu, K.; Berry, J.J. Defect Tolerance in Methylammonium Lead Triiodide Perovskite. *ACS Energy Lett.* **2016**, *1*, 360–366. [[CrossRef](#)]
16. Johnston, M.B.; Herz, L.M. Hybrid Perovskites for Photovoltaics: Charge-Carrier Recombination, Diffusion, and Radiative Efficiencies. *Acc. Chem. Res.* **2015**, *49*, 146–154. [[CrossRef](#)]
17. Brandt, R.E.; Poindexter, J.R.; Gorai, P.; Kurchin, R.C.; Hoye, R.L.Z.; Nienhaus, L.; Wilson, M.W.B.; Polizzotti, J.A.; Sereika, R.; Zaltauskas, R.; et al. Searching for “Defect-Tolerant” Photovoltaic Materials: Combined Theoretical and Experimental Screening. *Chem. Mater.* **2017**, *29*, 4667–4674. [[CrossRef](#)]
18. Pazos-Outón, L.M.; Szumilo, M.; Lamboll, R.; Richter, J.M.; Crespo-Quesada, M.; Abdi-Jalebi, M.; Beeson, H.J.; Vručinić, M.; Alsari, M.; Snaith, H.J.; et al. Photon recycling in lead iodide perovskite solar cells. *Science* **2016**, *351*, 1430–1433. [[CrossRef](#)] [[PubMed](#)]
19. Gan, Z.; Wen, X.; Chen, W.; Zhou, C.; Yang, S.; Cao, G.; Ghiggino, K.P.; Zhang, H.; Jia, B. The dominant energy transport pathway in halide perovskites: Photon recycling or carrier diffusion? *Adv. Energy Mater.* **2019**, *9*, 1900185. [[CrossRef](#)]
20. Wright, A.D.; Verdi, C.; Milot, R.L.; Eperon, G.E.; Pérez-Osorio, M.A.; Snaith, H.J.; Giustino, F.; Johnston, M.B.; Herz, L.M. Electron–phonon coupling in hybrid lead halide perovskites. *Nat. Commun.* **2016**, *7*, 11755. [[CrossRef](#)]
21. Zhao, T.Q.; Shi, W.; Xi, J.Y.; Wang, D.; Shuai, Z.G. Intrinsic and Extrinsic Charge Transport in CH₃NH₃PbI₃ Perovskites Predicted from First-Principles. *Sci. Rep.* **2016**, *6*, 19968. [[CrossRef](#)] [[PubMed](#)]
22. Kirchartz, T.; Markvart, T.; Rau, U.; Egger, D.A. Impact of Small Phonon Energies on the Charge-Carrier Lifetimes in Metal-Halide Perovskites. *J. Phys. Chem. Lett.* **2018**, *9*, 939–946. [[CrossRef](#)] [[PubMed](#)]
23. Motta, C.; Sanvito, S. Electron–Phonon Coupling and Polaron Mobility in Hybrid Perovskites from First Principles. *J. Phys. Chem. C* **2018**, *122*, 1361–1366. [[CrossRef](#)]

24. Frost, J.M.; Butler, K.T.; Walsh, A. Molecular ferroelectric contributions to anomalous hysteresis in hybrid perovskite solar cells. *APL Mater.* **2014**, *2*, 081506. [[CrossRef](#)]
25. Liu, S.; Zheng, F.; Koocher, N.Z.; Takenaka, H.; Wang, F.G.; Rappe, A.M. Ferroelectric Domain Wall Induced Band Gap Reduction and Charge Separation in Organometal Halide Perovskites. *J. Phys. Chem. Lett.* **2015**, *6*, 693–699. [[CrossRef](#)] [[PubMed](#)]
26. Zhu, X.-Y.; Podzorov, V. Charge Carriers in Hybrid Organic–Inorganic Lead Halide Perovskites Might Be Protected as Large Polarons. *J. Phys. Chem. Lett.* **2015**, *6*, 4758–4761. [[CrossRef](#)] [[PubMed](#)]
27. Zheng, F.; Tan, L.Z.; Liu, S.; Rappe, A.M. Rashba spin–orbit coupling enhanced carrier lifetime in $\text{CH}_3\text{NH}_3\text{PbI}_3$. *Nano Lett.* **2015**, *15*, 7794. [[CrossRef](#)] [[PubMed](#)]
28. Myung, C.W.; Javaid, S.; Kim, K.S.; Lee, G. Rashba–Dresselhaus effect in inorganic/organic lead iodide perovskite interfaces. *ACS Energy Lett.* **2018**, *3*, 1294. [[CrossRef](#)]
29. Zhang, X.; Shen, J.-X.; Van de Walle, C.G. Three-Dimensional Spin Texture in Hybrid Perovskites and Its Impact on Optical Transitions. *J. Phys. Chem. Lett.* **2018**, *9*, 2903–2908. [[CrossRef](#)]
30. Dresselhaus, G.; Kip, A.F.; Kittel, C. Spin-Orbit Interaction and the Effective Masses of Holes in Germanium. *Phys. Rev. B* **1954**, *95*, 568–569. [[CrossRef](#)]
31. Rashba, E.I. Properties of semiconductors with an extremum loop. 1. Cyclotron and combinational resonance in a magnetic field perpendicular to the plane of the loop. *Phys. Solid State* **1960**, *2*, 1224–1238.
32. Awschalom, D.D.; Loss, D.; Samarth, N. (Eds.) *Semiconductor Spintronics and Quantum Computation*; Springer: Berlin/Heidelberg, Germany; New York, NY, USA, 2002.
33. Protesescu, L.; Yakunin, S.; Bodnarchuk, M.I.; Krieg, F.; Caputo, R.; Hendon, C.H.; Yang, R.X.; Walsh, A.; Kovalenko, M.V. Nanocrystals of Cesium Lead Halide Perovskites (CsPbX_3 , X = Cl, Br, and I): Novel Optoelectronic Materials Showing Bright Emission with Wide Color Gamut. *Nano Lett.* **2015**, *15*, 3692–3696. [[CrossRef](#)] [[PubMed](#)]
34. Triana, M.A.; Hsiang, E.-L.; Zhang, C.; Dong, Y.; Wu, S.-T. Luminescent Nanomaterials for Energy-Efficient Display and Healthcare. *ACS Energy Lett.* **2022**, *7*, 1001–1020. [[CrossRef](#)]
35. Zhang, C.; He, Z.; Chen, H.; Zhou, L.; Tan, G.; Wu, S.-T.; Dong, Y. Light diffusing, down-converting perovskite-on-polymer microspheres. *J. Mater. Chem. C* **2019**, *7*, 6527–6533. [[CrossRef](#)]
36. Feng, X.; Sheng, Y.; Ma, K.; Xing, F.; Liu, C.; Yang, X.; Qian, H.; Zhang, S.; Di, Y.; Liu, Y.; et al. Multi-Level Anti-Counterfeiting and Optical Information Storage Based on Luminescence of Mn-Doped Perovskite Quantum Dots. *Adv. Opt. Mater.* **2022**, *10*, 2200706. [[CrossRef](#)]
37. Kim, M.; Im, J.; Freeman, A.J.; Ihm, J.; Jin, H. Switchable $S = 1/2$ and $J = 1/2$ Rashba bands in ferroelectric halide perovskites. *Proc. Natl. Acad. Sci. USA* **2014**, *111*, 6900. [[CrossRef](#)] [[PubMed](#)]
38. Etienne, T.; Mosconi, E.; De Angelis, F. Dynamical Rashba Band Splitting in Hybrid Perovskites Modeled by Local Electric Fields. *J. Phys. Chem. C* **2018**, *122*, 124–132. [[CrossRef](#)]
39. Hu, S.; Gao, H.; Qi, Y.; Tao, Y.; Li, Y.; Reimers, J.R.; Bokdam, M.; Franchini, C.; Di Sante, D.; Stroppa, A.; et al. Dipole Order in Halide Perovskites: Polarization and Rashba Band Splittings. *J. Phys. Chem. C* **2017**, *121*, 23045–23054. [[CrossRef](#)]
40. Stroppa, A.; Di Sante, D.; Barone, P.; Bokdam, M.; Kresse, G.; Franchini, C.; Whangbo, M.-H.; Picozzi, S. Tunable ferroelectric polarization and its interplay with spin–orbit coupling in tin iodide perovskites. *Nat. Commun.* **2014**, *5*, 5900. [[CrossRef](#)]
41. Manser, J.S.; Christians, J.A.; Kamat, P.V. Intriguing Optoelectronic Properties of Metal Halide Perovskites. *Chem. Rev.* **2016**, *116*, 12956–13008. [[CrossRef](#)]
42. Giovanni, D.; Ma, H.; Chua, J.; Gratzel, M.; Ramesh, R.; Mhaisalkar, S.; Mathews, N.; Sum, T.C. Highly spin-polarized carrier dynamics and ultra large photoinduced magnetization in $\text{CH}_3\text{NH}_3\text{PbI}_3$ perovskite thin films. *Nano Lett.* **2015**, *15*, 1553. [[CrossRef](#)] [[PubMed](#)]
43. Niesner, D.; Wilhelm, M.; Levchuk, I.; Osvet, A.; Shrestha, S.; Batentschuk, M.; Brabec, C.; Fauster, T. Giant Rashba splitting in $\text{CH}_3\text{NH}_3\text{PbBr}_3$ organic–inorganic perovskite. *Phys. Rev. Lett.* **2016**, *117*, 126401. [[CrossRef](#)] [[PubMed](#)]
44. Wang, Y.; Zha, Y.; Bao, C.; Hu, F.; Di, Y.; Liu, C.; Xing, F.; Xu, X.; Wen, X.; Gan, Z.; et al. Monolithic 2D Perovskites Enabled Artificial Photonic Synapses for Neuromorphic Vision Sensors. *Adv. Mater.* **2024**, *36*, e2311524. [[CrossRef](#)] [[PubMed](#)]
45. Zha, Y.; Wang, Y.; Sheng, Y.; Zhang, X.; Shen, X.; Xing, F.; Liu, C.; Di, Y.; Cheng, Y.; Gan, Z. Stable and broadband photodetectors based on 3D/2D perovskite heterostructures with surface passivation. *Appl. Phys. Lett.* **2022**, *121*, 191904. [[CrossRef](#)]
46. Chen, Y.; Sun, Y.; Peng, J.; Tang, J.; Zheng, K.; Liang, Z. 2D Ruddlesden–Popper Perovskites for Optoelectronics. *Adv. Mater.* **2018**, *30*, 1703487. [[CrossRef](#)] [[PubMed](#)]
47. Dou, L.; Wong, A.B.; Yu, Y.; Lai, M.; Kornienko, N.; Eaton, S.W.; Fu, A.; Bischak, C.G.; Ma, J.; Ding, T.; et al. Atomically thin two-dimensional organic-inorganic hybrid perovskites. *Science* **2015**, *349*, 1518–1521. [[CrossRef](#)] [[PubMed](#)]
48. Blancon, J.-C.; Tsai, H.; Nie, W.; Stoumpos, C.C.; Pedesseau, L.; Katan, C.; Kepenekian, M.; Soe, C.M.M.; Appavoo, K.; Sfeir, M.Y.; et al. Extremely efficient internal exciton dissociation through edge states in layered 2D perovskites. *Science* **2017**, *355*, 1288–1292. [[CrossRef](#)] [[PubMed](#)]
49. Tsai, H.; Nie, W.; Blancon, J.-C.; Stoumpos, C.C.; Asadpour, R.; Harutyunyan, B.; Neukirch, A.J.; Verduzco, R.; Crochet, J.J.; Tretiak, S.; et al. High-efficiency two-dimensional Ruddlesden–Popper perovskite solar cells. *Nature* **2016**, *536*, 312–316. [[CrossRef](#)] [[PubMed](#)]
50. Kumagai, M.; Takagahara, T. Excitonic and nonlinear-optical properties of dielectric quantum-well structures. *Phys. Rev. B* **1989**, *40*, 12359–12381. [[CrossRef](#)]
51. Cao, D.H.; Stoumpos, C.C.; Farha, O.K.; Hupp, J.T.; Kanatzidis, M.G. 2D Homologous Perovskites as Light-Absorbing Materials for Solar Cell Applications. *J. Am. Chem. Soc.* **2015**, *137*, 7843–7850. [[CrossRef](#)]

52. Ahmad, S.; Fu, P.; Yu, S.; Yang, Q.; Liu, X.; Wang, X.; Wang, X.; Guo, X.; Li, C. Dion-Jacobson phase 2D layered perovskites for solar cells with ultrahigh stability. *Joule* **2019**, *3*, 794. [[CrossRef](#)]
53. Ren, H.; Yu, S.; Chao, L.; Xia, Y.; Sun, Y.; Zuo, S.; Li, F.; Niu, T.; Yang, Y.; Ju, H.; et al. Efficient and stable Ruddlesden–Popper perovskite solar cell with tailored interlayer molecular interaction. *Nat. Photonics* **2020**, *14*, 154–163. [[CrossRef](#)]
54. Gan, Z.; Cheng, Y.; Chen, W.; Loh, K.P.; Jia, B.; Wen, X. Photophysics of 2D organic–inorganic hybrid lead halide perovskites: Progress, debates, and challenges. *Adv. Sci.* **2021**, *8*, 2001843. [[CrossRef](#)] [[PubMed](#)]
55. Bychkov, Y.A.; Rashba, E.I. Properties of a 2D Electron-Gas with Lifted Spectral Degeneracy. *JETP Lett.* **1984**, *39*, 78–81.
56. Nitta, J.; Akazaki, T.; Takayanagi, H.; Enoki, T. Gate Control of Spin-Orbit Interaction in an Inverted In_{0.53}Ga_{0.47}As/In_{0.52}Al_{0.48}As Heterostructure. *Phys. Rev. Lett.* **1997**, *78*, 1335–1338. [[CrossRef](#)]
57. King, P.D.; Hatch, R.C.; Bianchi, M.; Ovsyannikov, R.; Lupulescu, C.; Landolt, G.; Slomski, B.; Dil, J.H.; Guan, D.; Mi, J.L.; et al. Large Tunable Rashba Spin Splitting of a Two-Dimensional Electron Gas in Bi₂Se₃. *Phys. Rev. Lett.* **2011**, *107*, 096802. [[CrossRef](#)] [[PubMed](#)]
58. Lesne, E.; Fu, Y.; Oyarzun, S.; Rojas-Sánchez, J.C.; Vaz, D.C.; Naganuma, H.; Sicoli, G.; Attané, J.-P.; Jamet, M.; Jacquet, E.; et al. Highly efficient and tunable spin-to-charge conversion through Rashba coupling at oxide interfaces. *Nat. Mater.* **2016**, *15*, 1261–1266. [[CrossRef](#)] [[PubMed](#)]
59. Zhai, Y.; Baniya, S.; Zhang, C.; Li, J.; Haney, P.; Sheng, C.-X.; Ehrenfreund, E.; Vardeny, Z.V. Giant Rashba splitting in 2D organic-inorganic halide perovskites measured by transient spectroscopies. *Sci. Adv.* **2017**, *3*, e1700704. [[CrossRef](#)] [[PubMed](#)]
60. Todd, S.B.; Riley, D.B.; Binai-Motlagh, A.; Clegg, C.; Ramachandran, A.; March, S.A.; Hoffman, J.M.; Hill, I.G.; Stoumpos, C.C.; Kanatzidis, M.G.; et al. Detection of Rashba spin splitting in 2D organic-inorganic perovskite via precessional carrier spin relaxation. *APL Mater.* **2019**, *7*, 081116. [[CrossRef](#)]
61. Park, I.-H.; Zhang, Q.; Kwon, K.C.; Zhu, Z.; Yu, W.; Leng, K.; Giovanni, D.; Choi, H.S.; Abdelwahab, I.; Xu, Q.-H.; et al. Ferroelectricity and Rashba Effect in a Two-Dimensional Dion-Jacobson Hybrid Organic–Inorganic Perovskite. *J. Am. Chem. Soc.* **2019**, *141*, 15972–15976. [[CrossRef](#)]
62. Jana, M.K.; Song, R.; Liu, H.; Khanal, D.R.; Janke, S.M.; Zhao, R.; Liu, C.; Vardeny, Z.V.; Blum, V.; Mitzi, D.B. Organic-to-inorganic structural chirality transfer in a 2D hybrid perovskite and impact on Rashba-Dresselhaus spin-orbit coupling. *Nat. Commun.* **2020**, *11*, 4699. [[CrossRef](#)] [[PubMed](#)]
63. Kagdada, H.L.; Gupta, S.K.; Sahoo, S.; Singh, D.K. Mobility driven thermoelectric and optical properties of two-dimensional halide-based hybrid perovskites: Impact of organic cation rotation. *Phys. Chem. Chem. Phys.* **2022**, *24*, 8867–8880. [[CrossRef](#)] [[PubMed](#)]
64. Zhou, B.; Liang, L.; Ma, J.; Li, J.; Li, W.; Liu, Z.; Li, H.; Chen, R.; Li, D. Thermally Assisted Rashba Splitting and Circular Photogalvanic Effect in Aqueously Synthesized 2D Dion–Jacobson Perovskite Crystals. *Nano Lett.* **2021**, *21*, 4584–4591. [[CrossRef](#)] [[PubMed](#)]
65. Mitzi, D.B. Synthesis, structure and properties of organic-inorganic perovskites and related materials. *Prog. Inorg. Chem.* **1999**, *48*, 121.
66. Shao, Y.; Gao, W.; Yan, H.; Li, R.; Abdelwahab, I.; Chi, X.; Rogée, L.; Zhuang, L.; Fu, W.; Lau, S.P.; et al. Unlocking surface octahedral tilt in two-dimensional Ruddlesden–Popper perovskites. *Nat. Commun.* **2022**, *13*, 138. [[CrossRef](#)] [[PubMed](#)]
67. Singh, S.; Gong, W.; Stevens, C.E.; Hou, J.; Singh, A.; Zhang, H.; Anantharaman, S.B.; Mohite, A.D.; Hendrickson, J.R.; Yan, Q.; et al. Valley-Polarized Interlayer Excitons in 2D Chalcogenide–Halide Perovskite–van der Waals Heterostructures. *ACS Nano* **2023**, *17*, 7487–7497. [[CrossRef](#)] [[PubMed](#)]
68. Yin, J.; Maity, P.; Xu, L.; El-Zohry, A.M.; Li, H.; Bakr, O.M.; Brédas, J.-L.; Mohammed, O.F. Layer-Dependent Rashba Band Splitting in 2D Hybrid Perovskites. *Chem. Mater.* **2018**, *30*, 8538–8545. [[CrossRef](#)]
69. Liu, B.; Gao, H.; Meng, C.; Ye, H. The Rashba effect in two-dimensional hybrid perovskites: The impacts of halogens and surface ligands. *Phys. Chem. Chem. Phys.* **2022**, *24*, 27827–27835. [[CrossRef](#)] [[PubMed](#)]
70. Efros, A.L.; Brus, L.E. Nanocrystal Quantum Dots: From Discovery to Modern Development. *ACS Nano* **2021**, *15*, 6192–6210. [[CrossRef](#)]
71. Geiregat, P.; Rodá, C.; Tanghe, I.; Singh, S.; Di Giacomo, A.; Lebrun, D.; Grimaldi, G.; Maes, J.; Van Thourhout, D.; Moreels, I.; et al. Localization-limited exciton oscillator strength in colloidal CdSe nanoplatelets revealed by the optically induced stark effect. *Light Sci. Appl.* **2021**, *10*, 112. [[CrossRef](#)]
72. Swift, M.W.; Lyons, J.L.; Efros, A.L.; Sercel, P.C. Rashba exciton in a 2D perovskite quantum dot. *Nanoscale* **2021**, *13*, 16769. [[CrossRef](#)] [[PubMed](#)]
73. Li, J.; Guo, Z.; Qin, Y.; Liu, R.; He, Y.; Zhu, X.; Xu, F.; He, T. Rashba Effect and Spin-Dependent Excitonic Properties in Chiral Two-Dimensional/Three-Dimensional Composite Perovskite Films. *J. Phys. Chem. Lett.* **2023**, *14*, 11697–11703. [[CrossRef](#)] [[PubMed](#)]
74. Thouin, F.; Golub, L.; Lomakina, F.; Bel’kov, V.; Olbrich, P.; Stachel, S.; Caspers, I.; Griesbeck, M.; Kugler, M.; Hirmer, M.J.; et al. Phonon coherences reveal the polaronic character of excitons in two-dimensional lead halide perovskites. *Nat. Mater.* **2019**, *18*, 349–356. [[CrossRef](#)] [[PubMed](#)]
75. Lechner, V.; Golub, L.E.; Lomakina, F.; Bel’kov, V.V.; Olbrich, P.; Stachel, S.; Caspers, I.; Griesbeck, M.; Kugler, M.; Hirmer, M.J.; et al. Spin and orbital mechanisms of the magnetogyrotropic photogalvanic effects in GaAs/Al_xGa_{1-x}As quantum well structures. *Phys. Rev. B* **2011**, *83*, 155313. [[CrossRef](#)]
76. Lee, J.S.; Schober, G.A.H.; Bahramy, M.S.; Murakawa, H.; Onose, Y.; Arita, R.; Nagaosa, N.; Tokura, Y. Optical Response of Relativistic Electrons in the Polar BiTeI Semiconductor. *Phys. Rev. Lett.* **2011**, *107*, 117401. [[CrossRef](#)] [[PubMed](#)]
77. Yuan, H.; Wang, X.; Lian, B.; Zhang, H.; Fang, X.; Shen, B.; Xu, G.; Xu, Y.; Zhang, S.-C.; Hwang, H.Y.; et al. Generation and electric control of spin–valley-coupled circular photogalvanic current in WSe₂. *Nat. Nanotechnol.* **2014**, *9*, 851–857. [[CrossRef](#)] [[PubMed](#)]

78. Dong, Y.; Zhang, Y.; Li, X.; Feng, Y.; Zhang, H.; Xu, J. Chiral perovskites: Promising materials toward next-generation optoelectronics. *Small* **2019**, *15*, 1902237. [[CrossRef](#)] [[PubMed](#)]
79. Dang, Y.; Liu, X.; Cao, B.; Tao, X. Chiral halide perovskite crystals for optoelectronic applications. *Matter* **2021**, *4*, 794–820. [[CrossRef](#)]
80. Ma, J.; Wang, H.; Li, D. Recent Progress of Chiral Perovskites: Materials, Synthesis, and Properties. *Adv. Mater.* **2021**, *33*, 2008785. [[CrossRef](#)]
81. Zhang, X.; Liu, X.; Li, L.; Ji, C.; Yao, Y.; Luo, J. Great Amplification of Circular Polarization Sensitivity via Heterostructure Engineering of a Chiral Two-Dimensional Hybrid Perovskite Crystal with a Three-Dimensional MAPbI₃ Crystal. *ACS Cent. Sci.* **2021**, *7*, 1261–1268. [[CrossRef](#)]
82. Huang, P.-J.; Taniguchi, K.; Shigefuji, M.; Kobayashi, T.; Matsubara, M.; Sasagawa, T.; Sato, H.; Miyasaka, H. Chirality-Dependent Circular Photogalvanic Effect in Enantiomorphic 2D Organic–Inorganic Hybrid Perovskites. *Adv. Mater.* **2021**, *33*, 2008611. [[CrossRef](#)] [[PubMed](#)]
83. Liu, T.; Shi, W.; Tang, W.; Liu, Z.; Schroeder, B.C.; Fenwick, O.; Fuchter, M.J. High Responsivity Circular Polarized Light Detectors based on Quasi Two-Dimensional Chiral Perovskite Films. *ACS Nano* **2022**, *16*, 2682–2689. [[CrossRef](#)] [[PubMed](#)]
84. Ward, M.D.; Shi, W.; Gasparini, N.; Nelson, J.; Wade, J.; Fuchter, M.J. Materials for optical, magnetic and electronic devices. *J. Mater. Chem. C* **2022**, *10*, 10452. [[CrossRef](#)] [[PubMed](#)]
85. Wang, J.; Lu, H.; Pan, X.; Xu, J.; Liu, H.; Liu, X.; Khanal, D.R.; Toney, M.F.; Beard, M.C.; Vardeny, Z.V. Spin-Dependent Photovoltaic and Photogalvanic Responses of Optoelectronic Devices Based on Chiral Two-Dimensional Hybrid Organic–Inorganic Perovskites. *ACS Nano* **2021**, *15*, 588–595. [[CrossRef](#)]
86. Fan, C.-C.; Han, X.-B.; Liang, B.-D.; Shi, C.; Miao, L.-P.; Chai, C.-Y.; Liu, C.-D.; Ye, Q.; Zhang, W. Chiral Rashba Ferroelectrics for Circularly Polarized Light Detection. *Adv. Mater.* **2022**, *34*, e2204119. [[CrossRef](#)]

Disclaimer/Publisher’s Note: The statements, opinions and data contained in all publications are solely those of the individual author(s) and contributor(s) and not of MDPI and/or the editor(s). MDPI and/or the editor(s) disclaim responsibility for any injury to people or property resulting from any ideas, methods, instructions or products referred to in the content.